Journal of Luminescence xxx (xxxx) 120803

Contents lists available at ScienceDirect

Journal of Luminescence

journal homepage: www.elsevier.com/locate/jlumin

Scratching of metallized polymer films by Vickers indenter as a method for controlled production of SERS-active metasurfaces

N.P. Kovalets [a, b, *], E.P. Kozhina [a, b, c], I.V. Razumovskaya [a], A.I. Arzhanov [a, b], A.V. Naumov [a, b, d]

[a] Moscow Pedagogical State University (MPGU), Malaya Pirogovskaya St. 29, 119992, Moscow, Russia
[b] P.N. Lebedev Physical Institute of the Russian Academy of Sciences, Troitsk Branch, Fizicheskaya Str. 11, 108840, Moscow, Troitsk, Russia
[c] Skolkovo Institute of Science and Technology, Bolshoy Boulevard, 30, p.1, 12120, Moscow, Russia
[d] Institute for Spectroscopy RAS, 5 Fizicheskaya Str., 108840, Moscow, Troitsk, Russia

ARTICLE INFO

Keywords:
SERS
Microcracks
Microscratches
Metallized surface
Vickers indenter
Atomic force microscopy

ABSTRACT

The opportunities of a system of parallel microscratches drowed on a PET film metallized with silver and copper using a Vickers indenter as an active Surface-enhanced Raman spectroscopy (SERS) or Photoluminescence-enhanced surface have been investigated. It is shown that the enhancement of the SERS signal for rhodomine is proportional to the total length of microscratches in the laser spot and increases after their application due to the relaxation of the polymer backing. The results of the microscratch geometry analysis by an atomic force microscopy and scanning electron microscopy methods indicate the probability of the location of "hot points" along the "dumps" of metal along the shores of scratches, as well as on nanoroughnesses along their inner walls.

1. Introduction

To date, photoluminescence (PL) and Raman spectroscopies (including enhanced PL and Surface Enhanced Raman spectroscopy, SERS) has been increasingly used not only in laboratories but also in real applications [1–4]. This has led to active development of portable spectrometers and increased interest in enhancing nanostructured surfaces, including those with ordered geometry [5–7]. The ordered geometry of enhancing surfaces provides repeatability and stability of the SERS signal, which is particularly important for conducting express diagnostics of substance composition in non-laboratory conditions [8]. In the case of a statistical distribution of the active surface elements, it is desirable for these elements to be significantly smaller than the laser spot size, allowing statistical methods to be applied to them rather than a larger number of measurements.

As known, the enhancement of the SERS signal of a substance is determined by its position in direct proximity to the tips and roughness of plasmonic nanostructures (tip hot spots) or within the gaps between them (gap hot spots) [9–12]. Just the signal from the molecule located in the region with the most intense local electric field will dominate in the recorded spectrum [13]. Significant progress has been made in studying the dependence of SERS signal enhancement on the shape, size, and chemical composition of plasmonic nanostructures on which the investigated substance is applied [14–17]. For example, the radius of curvature of the tip of a plasmonic nanostructure also affects the signal enhancement [18,19].

A detailed analysis of various SERS-active metasurfaces has been conducted in works [20,21].

Of particular interest is the dependence of the SERS signal intensity on the mutual arrangement of nanostructures [22]. The concentration of the local electric field within the gaps between neighboring nanostructures exhibits a clearly expressed dying exponential type with increasing distance between them [23]. There are several solutions for artificially placing the investigated molecule in the region with the most concentrated electric field within the gap between nanostructures. For example, when a solution of molecules is applied to a substrate with an array of vertically standing nanowires (NWs), upon drying of the solution under the action of capillary forces, neighboring NWs are leaning by its tips, forming bundles [24–27]. In this case, the molecules that have adsorbed onto the tips of the NWs are located in a localized gap between the tips of neighboring NWs, and accordingly, in a region with the most intense electric field [28]. For such a substrate, the condition for stable agglomeration of NWs by its tips is determined by an energy criterion similar to Griffith's criterion for cracks (a balance between elastic and surface energy), taking into account the relationship between the distance between the NWs, their length, and thickness

* Corresponding author. Moscow Pedagogical State University (MPGU), Malaya Pirogovskaya St. 29, 119992, Moscow, Russia.
E-mail address: np_kovalets@mail.ru (N.P. Kovalets).

https://doi.org/10.1016/j.jlumin.2024.120803
Received 17 January 2024; Received in revised form 22 May 2024; Accepted 16 July 2024
0022-2313/© 20XX

[29–31]. The distance between the tips of neighboring NWs can be additionally controlled by a magnetic field during the synthesis of layered NWs that include a ferromagnetic segment [32].

A number of studies have demonstrated the possibility of the SERS signal gain on nanostructures bound with nano- and microcracks. For example, such an effect was observed on nanocracks of the silk fibroin 40-nm gold coating, which were formed during the evaporation of gold on porous silk [33]. Numerical simulation confirmed the local electric fields gain at hot spots in the producing nanogaps. In Ref. [34] nanocracks were obtained on the metal surface, coated of polydimethylsiloxane, and the corresponding SERS signal gain of the order of 10^6.

In our previous study [35] it was demonstrated that the microcracks system on a silver-metallized track-etched membrane (TM) serves as an active SERS surface. Comparing the SERS data with the surface conductivity data of the metallized surface [36] allowed us to conclude that the intensity of the SERS signal (considering the intensity of one of the peaks in the analyte's spectrum) is proportional to the total length of microcracks per unit area. This observation formed the basis for a patent on a method for determining the degree of local cracking of a plasmonic metal coating applied to a dielectric substrate [37].

However, the nature of the SERS signal enhancement on microcracks remains unknown. It can be hypothesized that the hotspots are either the boundary border of the microcracks (tip hot spot) or the nanogaps between their 'shores' (gap hot spot), or both factors are significant. In all cases, the effect is determined by the total length of microcracks in the laser spot. The polymer substrate also plays a significant role (in studies [29,36] – a track membrane based on polyethylene terephthalate (PET)): its mechanical relaxation after the completion of the microcrack system formation and the removal of tensile stress from the sample is accompanied with the enhancement of the SERS signal.

The aim of this study was to model microcracks, naturally occurring during the deformation of a metallized TM, as by a system of microscratches controllably applied to the metallized surface of a polymer film using the hardness gauge PMT-3M. This methodology allows for the variation of microscratch depth, length, distance (surface density), relative orientation, thereby simulating a statistically distributed system of natural microcracks with variation in their lengths. The dependence of the SERS signal intensity on the total length of microscratches in the laser spot can be easily established. In contrast to the case of randomly arranged microcracks of different lengths, there is no need for additional experimental methods. Moreover, there are additional experimental opportunities to clarify the nature of SERS signal enhancement.

At the same time, the obtained system of microscratches serves as a controlled SERS-active metasurface.

The method of sclerometry (microscratching) is actively used for a detailed analysis of the surface layers mechanical properties for various materials: the influence on the nature of their deformation and rupture of the load applied to the indenter, its orientation in the direction of scratching, scratching speed, temperature, etc. [38,39]. However, the purposes of the studies did not touch upon the problem of SERS-active surfaces. For example, in study [38] raised the problem of the surface of silicon texturing to increase the efficiency of solar cells. In Ref. [39] the task was the opposite: to substantiate the method of silicon carbide ceramics surface treatment for light space mirrors, for the needs of the nuclear industry, etc., with minimal roughness.

2. Materials and methods

For the main experiment, a 50 μm thick polyethylene terephthalate (PET) film with a silver coating was selected. The coating was applied using the thermal resistance method on a Saha vacuum deposition system. The thickness of the vaporized on layer (current 107 A, deposition time 40 s, pressure about 10^{-6} torr) was 50 nm, which corresponds to the thickness of a similar coating on PET in the study [35]. Copper was sprayed on PET at a current of 125 A. The thickness of the coating in both cases was determined by the deposition time, which was 40 s for the 50 nm layer, 80 s–100 nm.

Microscratches were manually applied using a Vickers indenter on the hardness gauge PMT-3M with a minimal load of 2 g at a scratch rate of approximately 0.5 mm/min. The Vickers indenter is a frustum of the tetrahedral pyramid with an angle of 136° between opposite faces. Scratches were obtained by penetration of the indenter into the surface layer and moving it parallel to one of the print diagonals (Fig. 1a).

The geometric parameters of the parallel microscratches system were evaluated using a Nikon Eclipse LV100 microscope (Japan) (Fig. 1b) and with the help of scanning electron microscopy (SEM) on the JSM-7401F device (JEOL, Japan).

The obtained 5 systems of parallel microscratches had the following parameters: the width of a microscratch, b_1, was of 10 μm, and the distance, b, between the centers of microscratches was of 2, 4, 6, 8, and 10 times the value of their width, b_1. The length of the microscratches certainly exceeded the diameter of the laser spot.

Cross-sectional profiles of microscratches were taken using an atomic force microscope (AFM) Ntegra Prima (NT-MDT, Russia) [40] with the following scanning parameters: cantilever NSG10, sample scanning speed 0.75 Hz per line, RMS Z = 0.25 nm for 1 s. Scanning areas in the experiment: 20 × 20 μm (500 × 500 pixels). The accuracy of scanning in the XY plane was comparable to the hardware function of the AFM (probe curvature radius of 10–15 nm). Filming was carried out in room conditions.

Aqueous solution of rhodamine (R6G) with a concentration of 10^{-4} M was used as an analyte for acquiring SERS spectra. For acquiring the normal Raman spectrum of R6G on a reference Al-foil, a concentration of 10^{-2} M was used. The volume of the applied droplet for both cases was of 3 μl. Spectra were acquired using a portable Raman spectrometer from ThermoFisher. The laser power was of 260 ± 10 mW. The comparative analysis of signal enhancement for various microscratch systems was conducted on the most prominent peaks of the spectrum located at 1364 и 1183 cm^{-1}.

3. Estimation of SERS efficiency factor (EF) on Cu- and Ag-surfaces with and without scratch

To establish the signal enhancement factor (EF), R6G was applied to a polymer coated with copper and silver, 50 nm thick, with and without a scratch. To effective estimation of the spreading of the analyte over the substrate, the technique of epi-luminescence microscopy was used. To estimate the wettability of substrate with an analyte, an experimental setup for an epi-luminescence microscope with a wide illumination

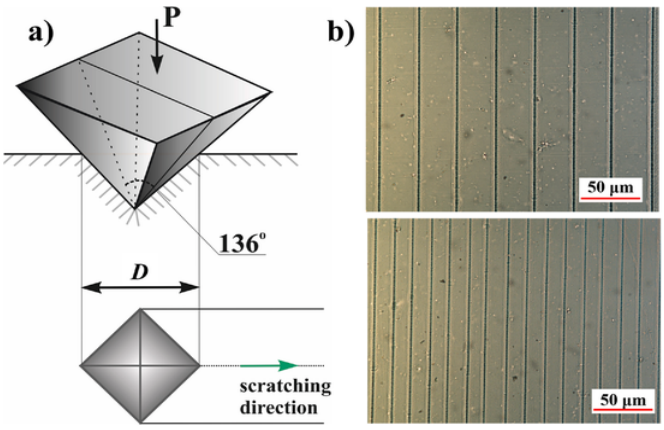

Fig. 1. Schematic drawing of a Vickers indenter (a) and photographs of microscratches in an optical microscope (b).

field was created in Ref. [41]. A semiconductor laser module (wavelength 525 nm, output power 200 mW) was used as a source of laser radiation. The laser radiation was focused onto an optical fiber, at the output of which it was defocused using an epi-lens into a wide and uniform spot of laser illumination (about 2 cm in diameter) for uniform irradiation of the entire area of the samples. Using a dividing plate and a system of lenses and an objective, the radiation from the sample was focused into an image on a PCO Sensicam SVGA CCD camera. To record luminescence from rhodamine, a broadband light filter and a high exposure time (1–3 s) on the camera were used.

The use of enhancing surfaces for measuring spectra in non-laboratory conditions is a necessary condition when analytes under study are at low concentrations. It is worth noting that the wavelengths of the exciting radiation source in portable spectrometers are chosen in the near red and IR range, since such sources weakly excite fluorescence. Copper nanostructures have a plasmon resonance in the IR, which arouses practical interest in their study due to the low cost of this metal. Fig. 2a shows the experimental spectra of R6G adsorbed on a polymer coated with copper and silver, 50 nm thick with a scratch. Including the spectra of the PET and the Raman spectrum of R6G on foil. The Raman spectrum of R6G on foil was pre-processed since the strong fluorescence background of the substance interfered. It can be seen that the spectrum of the polymer is not present in the SERS spectra of R6G adsorbed on a copper and silver surface with one scratch. Which, apparently, is due either to the dominant role of dumps during strengthening, or to the pulling of metal into the scratch.

Fig. 2b shows the experimental spectra of R6G adsorbed onto a polymer coated with copper and silver, 50 nm thick, with and without a scratch. To correctly compare two enhancing surfaces made from two different plasmonic metals, normalization of the intensity of the SERS spectra to the time of signal acquisition was introduced. The expediency of this normalization is determined by the linear dependence of the signal intensity on the accumulation time. Due to the fact that the portable spectrometer selects the signal acquisition time in automatic mode, this parameter cannot be ignored.

To estimate the enhancement factor of the SERS signal of R6G on a polymer metallized with silver and copper without and with a scratch, the spreading of an aqueous solution of R6G over the surface was assessed. Typical spreading images are presented in Table 1.

It is worth noting that the minimum spreading area of the aqueous solution is characteristic of foil, which is due to the low wettability of the surface. It is also worth noting that on foil, when a drop spreads, the molecules concentrate on the edges, forming a so-called coffee ring. The polymer metallized with copper and silver with a scratch is characterized by an ellipsoidal spreading pattern.

The formula for calculating the SERS (enhancement factor, EF) is as follows [42]:

$$EF_{SERS} = \frac{I_{SERS} \cdot N_{Raman}}{I_{Raman} \cdot N_{SERS}} \quad (1)$$

where I_{SERS} is the intensity of the SERS signal, N_{SERS} is the number of analyte molecules adsorbed on the surface of the substrate, I_{Raman} is the signal intensity in the absence of amplification, N_{Raman} is the number of analyte molecules adsorbed on the foil.

If the spreading area of the analyte (S) is known, then the formula for calculating the number of molecules in the laser-illuminated spot can be written as follows:

$$N = \frac{N_A \cdot C \cdot V \cdot A}{S} \quad (2)$$

where N_A is Avogadro's constant (6.022×10^{23} molecules/mol), C is the concentration of the solution (mol/l), V is the volume of the solution (l) – that was constant for both, Raman and SERS, cares, A is the area of the laser illumination spot (m^2), S is the surface area over which the molecules are distributed – the spreading area (m^2). This formula takes into account both the volumetric concentration of the solution and the area of spreading of the analysed substance over the surface. Then:

$$\frac{N_{Raman}}{N_{SERS}} = \frac{C_{Raman} \cdot S_{SERS}}{C_{SERS} \cdot S_{Raman}} \quad (3)$$

$$EF_{SERS} = \frac{I_{SERS} \cdot C_{Raman} \cdot S_{SERS}}{I_{Raman} \cdot C_{SERS} \cdot S_{Raman}} \quad (4)$$

To assess the signal intensity, the peak at 1181 cm^{-1} was considered. For a correct comparison, the R6G spectrum was also normalized to the signal accumulation time, which was 729 s. The concentration of R6G in terms of mol/L will be 0.000209 mol/L and 0.01 mol/L for application to enhancing surfaces and foils, respectively (detailed values are presented in Table 2). Thus, new controlled SERS-active metasurface has been achieved with EF is about 10^3.

4. The dependence of the SERS signal enhancement on the total length of microscratches in the laser spot

Earlier, we have demonstrated [36] that for microcracks in the silver-coated track membranes (TM), the intensity I of the SERS signal is directly proportional to the total length of microcracks in the laser emission spot. Let's verify the presence of a similar relationship in the case of microscratches on silver covering, considering the evident fact

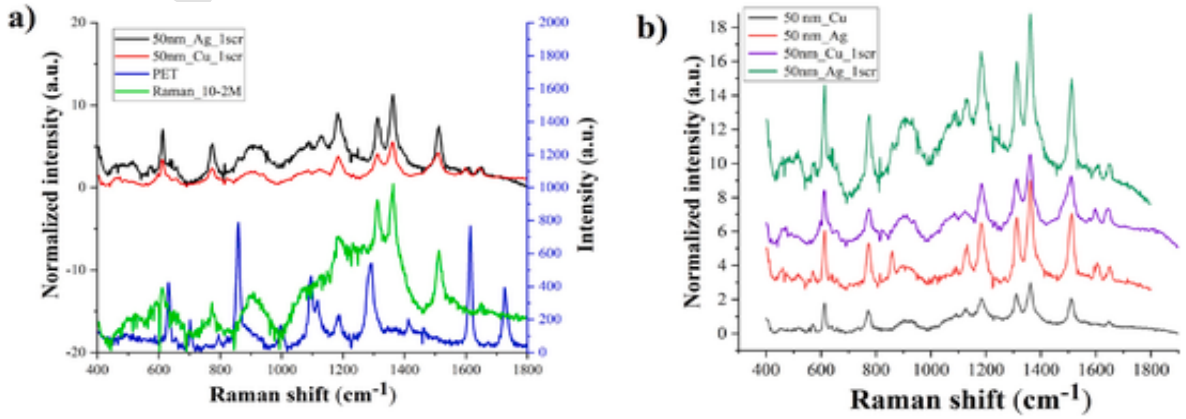

Fig. 2. a – Spectra of R6G molecules on Ag/PET and Cu/PET surfaces with one scratch, Raman spectra of PET and R6G on foil; b – Spectra of R6G molecules on Ag/PET and Cu/PET surfaces without scratches and with one scratch, normalized to the time of signal acquisition.

Table 1
Epi-luminescence microscopy of an aqueous solution of R6G on Cu- and Ag-coated films with and without a scratches.

	Without scratches	Scratched
Ag 50 nm/PET	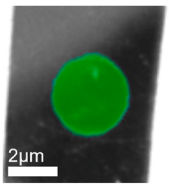	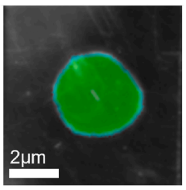
Cu 50 nm/PET	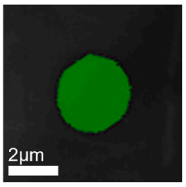	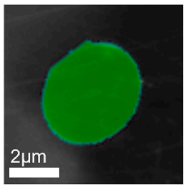
Reference Al foil	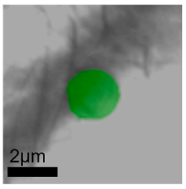	

Table 2
The spreading area of a drop of 3 μl solution of Rhodamine 6G at C = 10^{-4} M as well as SERS EF values.

Sample	Spreading area without a scratch, mm^2	Intensity, a.u.	EF	Spreading area with a scratch, mm^2	Intensity, a.u.	EF
Ag 50 nm/PET	11.03 mm^2	4	519	11.42 mm^2	9.1	1223
Cu 50nm/PET	10.48 mm^2	2.5	308	14.73 mm^2	3.8	659
Foil	S = 5.08 mm^2, IRaman = 0.8					

that the smaller the step size b, the greater the total length of scratches in the laser spot. The obtained effect of SERS signal enhancement is greater, the smaller the 'step' b between the scratches (Fig. 3).

Microscratches within the laser emission spot with a radius R form a system of parallel chords (Fig. 4).

A separate spectrum of rhodamine was recorded for a single scratch. In this case, the intensities of the corresponding peaks practically coincide with the experimental result for b = 100 μm. This means that the laser spot hits only one of the widely spaced scratches and has a diameter of about 100 μm.

In the case of '1' when one of the scratch systems coincides with the diameter of the spot, their total length L is equal to

$$L = 2\sum_{0}^{n_0}\sqrt{\left(R^2-(nb)^2\right)} = 2R\sum_{x=0}^{x=1}\sqrt{\left(1-x^2\right)} \quad (5)$$

where x = n/n_0, n_0 – the integer part R/b.

The case '2' in Fig. 4 is also easily calculated: symmetrical arrangement of scratches relative to the spot diameter in the absence of a scratch on the diameter itself. In a real experiment, some average value should be obtained for the magnitude of L. A primitive calculation shows that the arithmetical mean of the results from the '1' and '2' schemes can be used.

If the relative distance ('step') b/R, at which adjacent microscratches are located, is small enough, then in this case, doubling, tripling, etc., the 'step' simply means excluding some scratches corresponding to the next step b/R. Thus, the total length of microstretches in the laser spot will decrease by half, by a third, etc.

However, in our experiment, the value of the 'step' b is comparable to the radius of the spot R, and we are interested in comparing the calculated curve with the experimental results in the range of values from b/R = 1 to 0.1. In Fig. 5, in this range, the calculated curves 'L/2R – b/R' are shown for cases '1' and '2' in Fig. 4. On the same figure, the experimental points from Fig. 4 are plotted in the coordinates 'I/I_0 – b' in such a way that the values of the dimensionless coordinates L/2R and I/I_0 on the ordinate axis coincide. In this case, the values of I_0 for plotting the experimental points are taken as the intensity values obtained for a single scratch when L = 2R.

On the abscissa axis, two reference points are combined: 1) the zero point where b = 0 and b/R = 0; 2) points corresponding to L/2R = 1 and I/I_0 = 1, i.e., b/R = 1.7 (the result of averaging cases '1' and '2') and b = 100 μm. By comparing the values of b in micrometers and the corresponding value of b/R, the laser spot radius can be determined. It proved to be approximately 60 μm.

At distances b between scratches from 100 μm (10 values of scratch width b_1) to 60 μm (b = 6 b_1), the experimental points fall between the two calculated curves. The experimental point for b = 4 b_1 is also close to the calculated values.

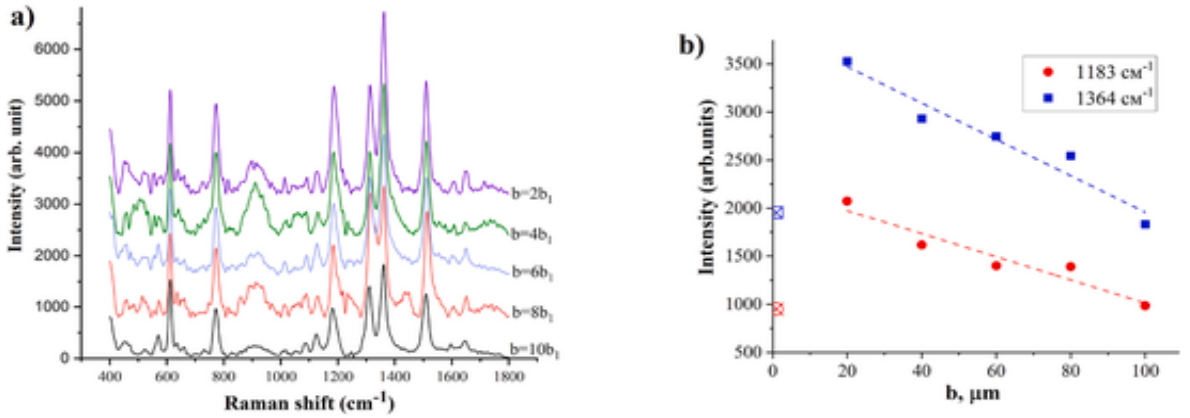

Fig. 3. a - the spectra of R6G molecules deposited on a system of scratches on a silver coating with different distances b; b - the dependence of the intensity of the SERS signal on the distance between the scratches for two peaks in the R6G spectrum. Two singles crossed out dots on Fig. 3b correspond to signals from a single scratch.

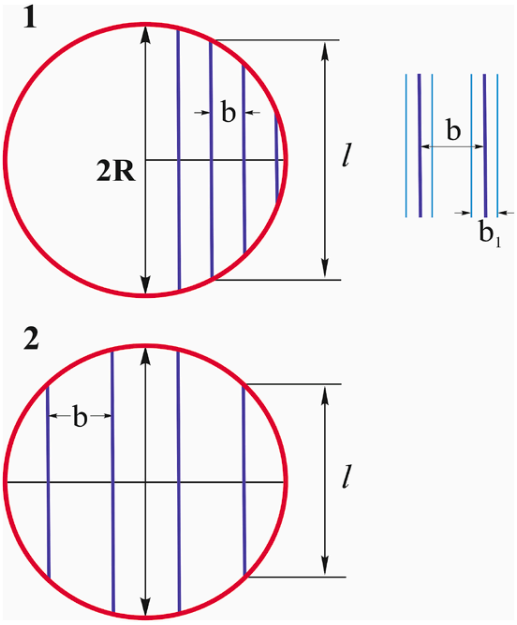

Fig. 4. Scheme for calculating the total length of scratches within the laser emission spot; b_1 – width of a scratch, b – distance between adjacent scratches.

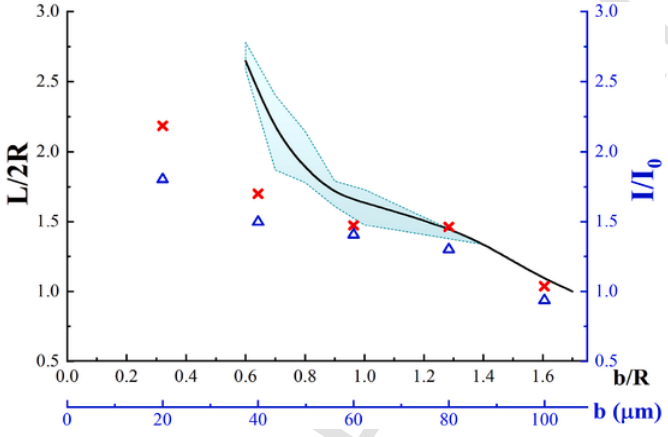

Fig. 5. Comparison of experimental values of the relative intensity I/I_0 of the SERS signal for two maxima of the rhodomine spectrum with the calculated values of the relative total average length of L/2R microscratches in the laser spot of radius R. The color-coded area around the calculation curve corresponds to all possible scratch locations in the laser spot.

The noticeable deviation of the experimental points from the calculated curve for $b = 2\,b_1$ is evidently observed. This can be explained by the fact that when the distance between scratches b becomes comparable to the width of the scratch b_1, their geometric parameters change (Fig. 6).

Thus, for microscratches, a direct proportional dependence between the signal intensity I and the total length of the scratches L in the laser spot is confirmed.

At the same time, analysis of the data in Fig. 6 shows that for practical use as a SERS-active substrate there is no point in creating a dense network of closely spaced scratches. A sufficient effect for intensity (2 times compared to a single scratch) is obtained in the range of values $b = (0.7–0.9)\,R$. At lower values of b, increasing the density of scratches in the laser spot gives an effect less than calculated due to the interaction of scratches and violations of their geometry. An effect approaching the calculated one can be obtained either by increasing the radius of the laser spot or by narrowing the scratches. You can also further increase the intensity of the SERS signal by using a grid of mutually perpendicular microscratches.

5. The nature of the enhancement of the SERS signal on microcracks and microscratches

The width of the scratch $b_1 = 10$ μm on the silver coating, according to the geometry of the Vickers indenter, corresponds to the depth of the indenter penetration $h = 1.4$ μm. For copper, these values are 7 μm and 1 μm, respectively, which is due to the greater microhardness of copper compared to silver. The h value is noticeably higher than the thickness of the metal coating (50 nm), which means that the scratch penetrates deeply into the surface layer of the polymer. However, AFM data show that after unloading, the scratch depth is significantly less than our estimate of h (Fig. 7).

In the case of a Vickers hardness for inorganic glass and a rigid polymer, the removal of the indenter induces almost instantaneous "jump up" of the print bottom due to elastic deformation, followed by its slow rise during relaxation [43].

It is possible that the relaxation of the polymer material at the bottom of the scratch and its narrowing can lead to an increase in the SERS signal over time. A similar time dependent effect was also observed for microcracks on metallized track membranes [35]. In the latter case, the macroscopic deformation of the entire previously elongated polymer substrate (track membrane) relaxed. In the case of microscratches, as in the case of microindentation, significant local shear and hydrostatic compression stresses relax after the indenter is removed, the relaxation process is more complex.

For the clarification of the role of the relaxation process of the polymer substrate, spectra were taken immediately after applying a microscratch to a silver and copper coating with a thickness of 100 nm and after 30 and 60 min (Figs. 7, 1b and 2b). The intensity was noticeably increased over time.

Figs. 7, 1a and 1b are also clearly visible "dumps" on the shores of the microscratches, which can bring in contribution to the amplification of the SERS signal. To determine the possible location of the "hot spots", a more detailed study of the microscratches geometry was carried out.

A SEM image of a microscratch on a 100 nm thick silver coating obtained is shown in Fig. 8. The figure shows periodic "waves" of metal on the walls of the microscratch, which arose during the movement of the indenter and may be the location of "hot spots" when the SERS effect occurs. Thus, it was desirable to record a set of successive cross sections of a microscratch using the AFM method. The results of this step-by-step shooting (Fig. 9) confirmed the presence of nanoirregularities on the internal walls of the microcrack. At the same time, nanoirregularities were recorded on the edges of the scratch.

6. Optical properties of luminophores in metallic microcracks: enhancing luminescence and light scattering

Within the scope of our research, we conducted a comprehensive investigation into the luminescent properties of rhodamine 6G on the surface of metallic cracks. CdSe/CdS/ZnS quantum dots were used as alternative luminophore. These quantum dots have already been studied in detail by our group in various studies [44,45]. Measurements were performed on a high-resolution optical microscopy setup using a 540 nm CW laser Hübner C-Wave as the excitation source.

Two solutions were prepared: rhodamine 6G in isopropanol with a concentration of 10^{-5} M in isopropanol and quantum dots 9.6 μg/ml in toluene. Both samples in a volume of 3 μl were applied to samples with metal microcracks. Using an epi-luminescent microscope in wide-field

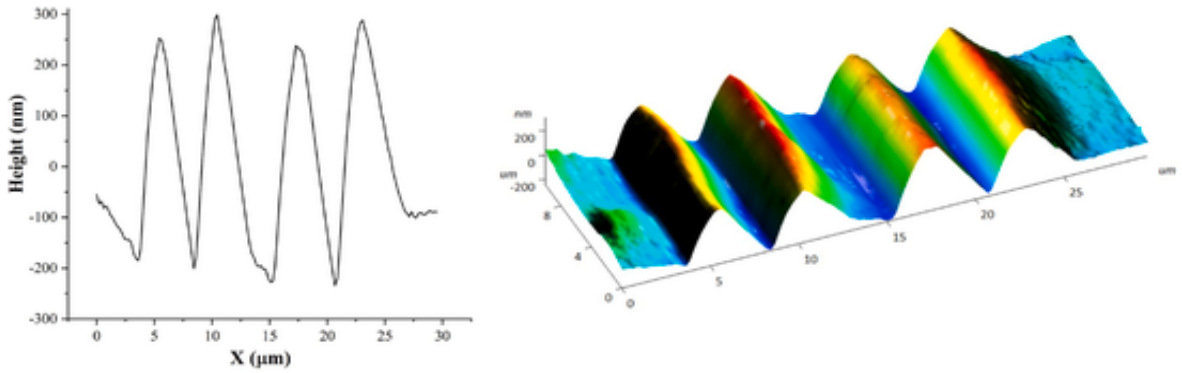

Fig. 6. Cross-sectional profile and 3D AFM image of two scratches with a distance between their centers $2b_1$.

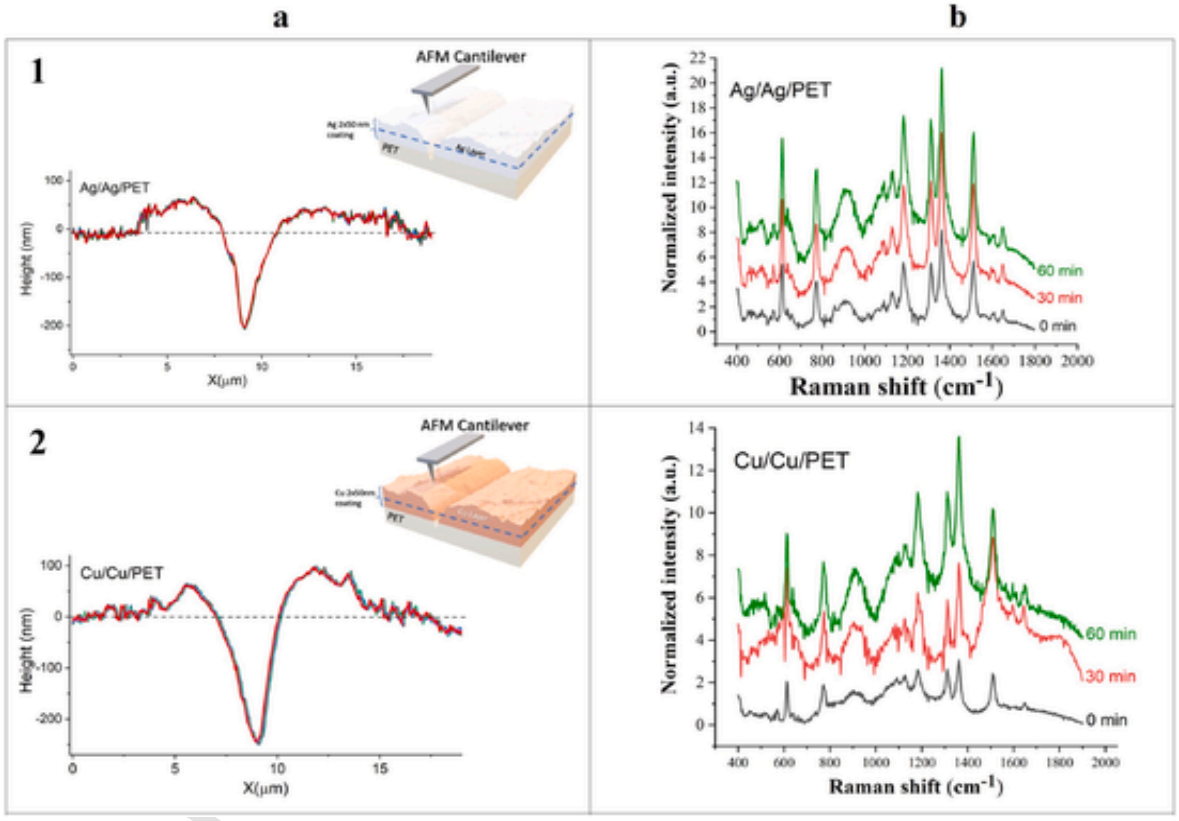

Fig. 7. a – profiles of the cross section of a microscratch immediately after its application to the silver (1a) and copper (2a) coating; b – changes in time of the R6G spectra on the corresponding coatings with single scratches.

mode, luminescent images of the crack area with the studied luminophores were obtained (Fig. 10.) at 100 μW excitation laser power in confocal spot.

The obtained data showed that for rhodamine 6G (Fig. 10 a), the luminescent profile in the crack region did not exhibit significant contrast compared to quantum dots CdSe/CdS/ZnS (Fig. 10 b) at the crack edge. The images show a statistical difference in the luminescence signal at the edge of the crack, which may indicate the presence of luminescence enhancement/quenching effects. This fact is confirmed by measurements of luminescence spectra in confocal mode. The luminescence spectra of rhodamine 6G and CdSe/CdS/ZnS QDs at the edge of a crack, as well as on the surface of a silver deposit of the same sample in the absence of defects, were measured (Fig. 11).

When analyzing the spectra, the maximum intensity values in the luminescence spectra were obtained. For rhodamine 6G (Fig. 11 a) the intensity was 28.9 and 41.1 a.u. for the case of recording the spectrum from an area at the edge of a microcrack and on a surface without defects, respectively. Considering that the concentration, as well as the power of the exciting laser radiation, is low enough to observe significant contributions of concentration and nonlinear effects, the quenching coefficient was estimated as the ratio of the maximum luminescence intensity and amounted to $Q_F = 0.7$.

In a similar way, the luminescence enhancement factor of CdSe/CdS/ZnS QDs (Fig. 11 b) was calculated - EF ≈ 2.75.

The observed differences in the obtained coefficients are associated with the presence of an effective distance between the surface plasmon

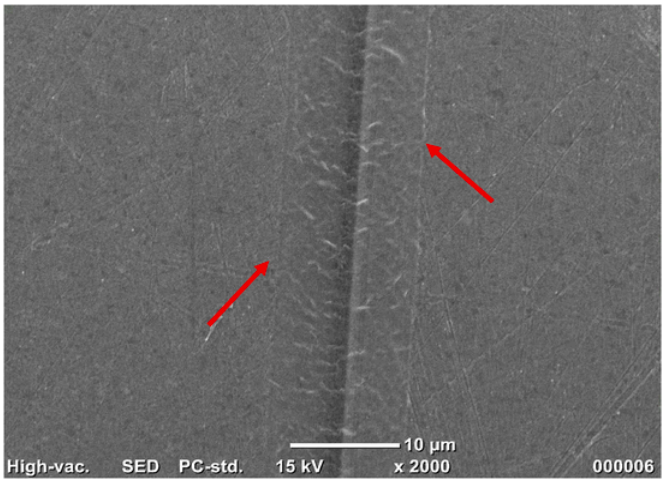

Fig. 8. SEM image of a microscratch on a 100 nm thick silver coating.

polariton and the emitter. For rhodamine, it is significantly small to observe the effect of enhancing luminescence, because molecules are adsorbed directly on the surface of the metal coating.

For the case of quantum dots, we can talk about the existence of such a distance at which an increase in the rate of spontaneous emission is observed due to the presence of organic ligands, as well as shells of a wide-gap semiconductor around the emitting CdSe core.

The obtained results represent an important step in understanding the mechanisms of luminescence enhancement and light scattering in nanostructured systems. A detailed description of the conducted experiments and data analysis is presented in article [46], where potential mechanisms influencing the optical properties and behavior of nanoparticles are also discussed.

7. Conclusion

The system of parallel microscratches on the silver and copper surface of metallized PET film is a SERS-active metasurface. The magnitude of the signal gain in the absence of microscratch interaction (up to the distance between them less than 4 values of the microscratch width) is proportional to the total length of the scratches in the laser spot. At a close distance between the scratches, their geometry is broken, and the new "double" structure shows greater increase than a single scratch, but less than two independent scratches. The study of the microscratches geometry by SEM and AFM methods showed the presence of the various nanoroughnesses both on the shores of scratches and on their walls. These disordered structures, statistically distributed along the length of the microscratch, can serve as "hot spots" (both tip hot spot and gap hot spot).

Mechanical relaxation processes in the polymer backing lead to a slight increase in the SERS signal, as in the case of the previously studied system of microcracks on a metallized track-etched membrane. The degree of influence of the polymer backing relaxation on the geometry of microcracks or microscratches is determined by the nature of the relaxing mechanical stress: uniaxial tension in the case of microcracks

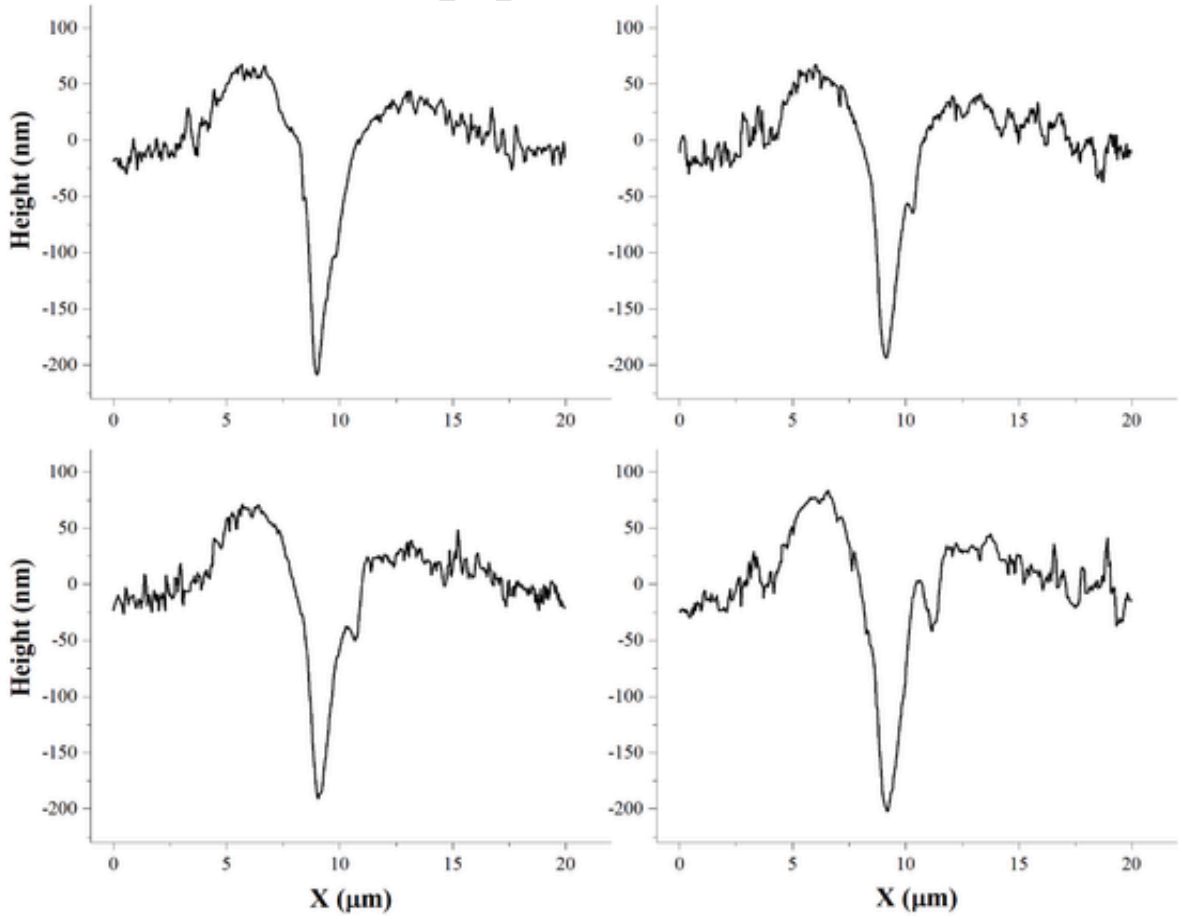

Fig. 9. Cross-sectional profiles of microscratches on a silver coating with a thickness of 100 nm, made with 5 μm step.

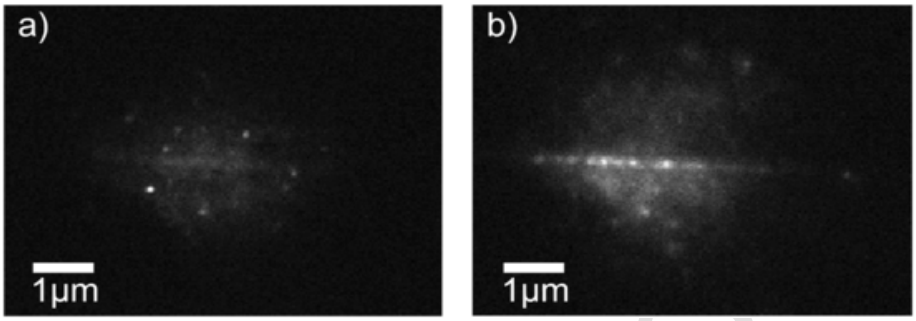

Fig. 10. Wide-field luminescence images of microcracks with Rhodamine 6G (a) and quantum dots CdSe/CdS/ZnS (b).

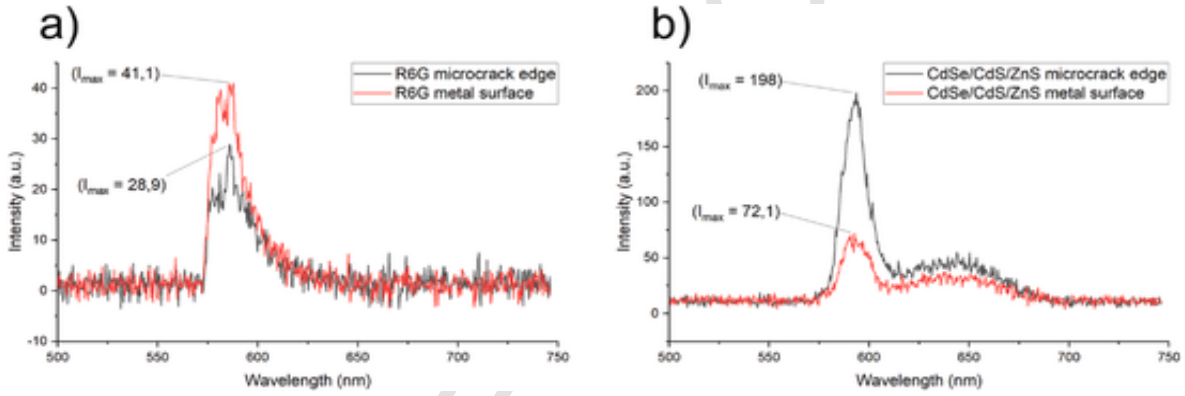

Fig. 11. Luminescence spectra of Rhodamine 6G (a) and quantum dots CdSe/CdS/ZnS (b) at metal surface and microcrack edge.

and large local compressive stresses in combination with shear in the case of microscratches. An experiment with enhancement of the role of polymer backing mechanical relaxation in changing the microscratches geometry seems prospective.

In conclusion, this article has examined the effects of luminescence enhancement in materials with defects, specifically at the edge of a microcrack. By conducting measurements of the luminescence spectra of Rhodamine 6G and CdSe/CdS/ZnS quantum dots, we have observed statistical differences in the signal, indicating the potential for luminescence enhancement.

Our findings allow for the estimation of the quenching (QF) and the enhancement factor (EF), which were determined to be 0.7 and 2.75, respectively. These values suggest significant enhancement effects, particularly in the case of CdSe/CdS/ZnS quantum dots.

Thus, our study expands our understanding of the influence of defects on the luminescent properties of materials and opens up new avenues for further research in this field.

CRediT authorship contribution statement

N.P. Kovalets: Writing – review & editing, Investigation, Formal analysis. **E.P. Kozhina:** Writing – original draft, Investigation. **I.V. Razumovskaya:** Writing – original draft, Supervision, Project administration. **A.I. Arzhanov:** Visualization, Software. **A.V. Naumov:** Supervision, Project administration.

Declaration of competing interest

The authors declare the following financial interests/personal relationships which may be considered as potential competing interests:Natalya Kovalets reports financial support was provided by Moscow State Pedagogical University. Natalya Kovalets reports a relationship with Moscow State Pedagogical University that includes:. If there are other authors, they declare that they have no known competing financial interests or personal relationships that could have appeared to influence the work reported in this paper.

Data availability

Data will be made available on request.

Acknowledgements

The research was carried out within the state assignment of The Ministry of Education of The Russian Federation “Physics of nanostructured materials and highly sensitive sensorics: synthesis, fundamental research and applications in photonics, life sciences, quantum and nanotechnology” (theme No. - 124031100005-5).

References

[1] A.V. Naumov, V.V. Utochnikova, Achievements and perspectives of luminescence at the All-Russian conference with international participation LUMOS-2024, Photonics Russia. 18 (3) (May 8 2024) 224–228, https://doi.org/10.22184/1993-7296.FRos.2024.18.3.224.228

[2] X. Huang, et al., Rapid detection of carbendazim residue in apple using surface-enhanced Raman scattering and coupled chemometric algorithm, Foods 11 (9) (Apr 28 2022), https://doi.org/10.3390/foods11091287.

[3] E.L. Holthoff, D.N. Stratis-Cullum, M.E. Hankus, A nanosensor for TNT detection based on molecularly imprinted polymers and surface enhanced Raman scattering, Sensors 11 (3) (2011) 2700–2714, https://doi.org/10.3390/s110302700.

[4] C. Camerlingo, M. Portaccio, R. Tate, M. Lepore, I. Delfino, Fructose and pectin detection in fruit-based food products by surface-enhanced Raman spectroscopy, Sensors 17 (4) (Apr 11 2017), https://doi.org/10.3390/s17040839.

[5] Q. Wang, et al., Tunable optical nanoantennas incorporating bowtie nanoantenna arrays with stimuli-responsive polymer, Sci. Rep. 5 (Dec 18 2015)

18567, https://doi.org/10.1038/srep18567.
[6] V. Pacheco-Peña, M. Beruete, A.I. Fernández-Domínguez, Y. Luo, M. Navarro-Cía, Description of bow-tie nanoantennas excited by localized emitters using conformal transformation, ACS Photonics 3 (7) (2016) 1223–1232, https://doi.org/10.1021/acsphotonics.6b00232.
[7] V. Suresh, L. Ding, A.B. Chew, F.L. Yap, Fabrication of large-area flexible SERS substrates by nanoimprint lithography, ACS Appl. Nano Mater. 1 (2) (2018) 886–893, https://doi.org/10.1021/acsanm.7b00295.
[8] M. Zhu, et al., Can "hot spots" Be stable enough for surface-enhanced Raman scattering? J. Phys. Chem. C 125 (24) (2021) 13443–13448, https://doi.org/10.1021/acs.jpcc.1c03321.
[9] E. Hao, G.C. Schatz, Electromagnetic fields around silver nanoparticles and dimers, J. Chem. Phys. 120 (1) (Jan 1 2004) 357–366, https://doi.org/10.1063/1.1629280.
[10] A.I. Perez-Jimenez, D. Lyu, Z. Lu, G. Liu, B. Ren, Surface-enhanced Raman spectroscopy: benefits, trade-offs and future developments, Chem. Sci. 11 (18) (Apr 14 2020) 4563–4577, https://doi.org/10.1039/d0sc00809e.
[11] E.C. Le Ru, M. Meyer, P.G. Etchegoin, Proof of single-molecule sensitivity in surface enhanced Raman scattering (SERS) by means of a two-analyte technique, J. Phys. Chem. B 110 (4) (Feb 2 2006) 1944–1948, https://doi.org/10.1021/jp054732v.
[12] E.P. Kozhina, S.N. Andreev, V.P. Tarakanov, S.A. Bedin, I.M. Doludenko, A.V. Naumov, Study of local fields of dendrite nanostructures in hot spots formed on SERS-active substrates produced via template-assisted synthesis, Bull. Russ. Acad. Sci. Phys. 84 (12) (2021) 1465–1468, https://doi.org/10.3103/s1062873820120205.
[13] Y. Sawai, B. Takimoto, H. Nabika, K. Ajito, K. Murakoshi, Observation of a small number of molecules at a metal nanogap arrayed on a solid surface using surface-enhanced Raman scattering, J. Am. Chem. Soc. 129 (6) (Feb 14 2007) 1658–1662, https://doi.org/10.1021/ja067034c.
[14] C.J. Orendorff, A. Gole, T.K. Sau, C.J. Murphy, Surface-enhanced Raman spectroscopy of self-assembled monolayers: sandwich architecture and nanoparticle shape dependence, Anal. Chem. 77 (10) (May 15 2005) 3261–3266, https://doi.org/10.1021/ac048176x.
[15] L. Rodriguez-Lorenzo, et al., Zeptomol detection through controlled ultrasensitive surface-enhanced Raman scattering, J. Am. Chem. Soc. 131 (13) (Apr 8 2009) 4616–4618, https://doi.org/10.1021/ja809418t.
[16] J. Beermann, S.M. Novikov, K. Leosson, S.I. Bozhevolnyi, Surface enhanced Raman imaging: periodic arrays and individual metal nanoparticles, Opt Express 17 (15) (Jul 20 2009) 12698–12705, https://doi.org/10.1364/oe.17.012698.
[17] S.E. Bell, M.R. McCourt, SERS enhancement by aggregated Au colloids: effect of particle size, Phys. Chem. Chem. Phys. 11 (34) (Sep 14 2009) 7455–7462, https://doi.org/10.1039/b906049a.
[18] C. Williams, D. Roy, Fabrication of gold tips suitable for tip-enhanced Raman spectroscopy, J. Vac. Sci. Technol. B: Microelectronics and Nanometer Structures Processing, Measurement, and Phenomena 26 (5) (2008) 1761–1764, https://doi.org/10.1116/1.2981078.
[19] A. Pavlič, Tip-Enhanced Raman Spectroscopy (TERS) under electrochemical conditions : towards the in situ characterization of functional nanomaterials. Theoretical And/or Physical Chemistry, Sorbonne Université, 2022.
[20] J. Langer, et al., Present and future of surface-enhanced Raman scattering, ACS Nano 14 (1) (Jan 28 2020) 28–117, https://doi.org/10.1021/acsnano.9b04224.
[21] G. Barbillon, Latest advances in metasurfaces for SERS and SEIRA sensors as well as photocatalysis, Int. J. Mol. Sci. 23 (18) (Sep 13 2022), https://doi.org/10.3390/ijms231810592.
[22] D. Lee, S. Yoon, Effect of nanogap curvature on SERS: a finite-difference time-domain study, J. Phys. Chem. C 120 (37) (2016) 20642–20650, https://doi.org/10.1021/acs.jpcc.6b01453.
[23] T. Chung, S.Y. Lee, E.Y. Song, H. Chun, B. Lee, Plasmonic nanostructures for nano-scale bio-sensing, Sensors 11 (11) (2011) 10907–10929, https://doi.org/10.3390/s111110907.
[24] E. Kozhina, et al., Ultrasensitive optical fingerprinting of biorelevant molecules by means of SERS-mapping on nanostructured metasurfaces, Biosensors 13 (1) (Dec 28 2022), https://doi.org/10.3390/bios13010046.
[25] S.J. Lee, A.R. Morrill, M. Moskovits, Hot spots in silver nanowire bundles for surface-enhanced Raman spectroscopy, J. Am. Chem. Soc. 128 (7) (Feb 22 2006) 2200–2201, https://doi.org/10.1021/ja0578350.
[26] E. Cara, et al., Influence of the long-range ordering of gold-coated Si nanowires on SERS, Sci. Rep. 8 (1) (Jul 27 2018) 11305, https://doi.org/10.1038/s41598-018-29641-x.
[27] M.S. Schmidt, J. Hubner, A. Boisen, Large area fabrication of leaning silicon nanopillars for surface enhanced Raman spectroscopy, Adv. Mater. 24 (10) (Mar 8 2012) OP11–O18, https://doi.org/10.1002/adma.201103496.
[28] E.P. Kozhina, et al., Ag-nanowire bundles with gap hot spots synthesized in track-etched membranes as effective SERS-substrates, Appl. Sci. 11 (4) (2021), https://doi.org/10.3390/app11041375.
[29] I.V. Razumovskaya, N.P. Kovalets, S.A. Bedin, Y.V. Grigor'ev, Agglomeration of nanowires on a substrate for surface-enhanced Raman scattering, J. Exp. Theor. Phys. 132 (5) (2021) 818–823, https://doi.org/10.1134/s1063776121050058.
[30] N.P. Kovalec, et al., Agglomeration of ensembles of silver nanowires, obtained by the method of template synthesis, Bull. Russ. Acad. Sci. Phys. 85 (8) (2021) 854–857, https://doi.org/10.3103/s1062873821080116.
[31] N.P. Kovalets, D.V. Panov, Y.A. Filippova, I.V. Razumovskaya, Point agglomeration of nickel and iron nanowires synthesized in the pores of track membranes, Bull. Russ. Acad. Sci. Phys. 85 (12) (2022) 1400–1403, https://doi.org/10.3103/s1062873821120145.
[32] Y.A. Filippova, A.V. Papugaeva, D.V. Panov,et, et al., Studying the Geometry and Physical Characteristics of FeNi Nanowires in Ferrofluids, Bull. Russ. Acad. Sci. Phys. 87 (2023) 1885–1889, https://doi.org/10.1134/S1062873823704142.
[33] J.H. Choi, M. Choi, T. Kang, T.S. Ho, S.H. Choi, K.M. Byun, Combination of porous silk fibroin substrate and gold nanocracks as a novel SERS platform for a high-sensitivity biosensor, Biosensors 11 (11) (Nov 6 2021), https://doi.org/10.3390/bios11110441.
[34] H. Mao, C. Qian, P. Lv, W. Wu, SERS-active substrates based on metallic nanocracks on PDMS. Presented at the in Proceedings of the 2011 6th IEEE International Conference on Nano/Micro Engineered and Molecular Systems, 2011.
[35] N.P. Kovalets, et al., Toward single-molecule surface-enhanced Raman scattering with novel type of metasurfaces synthesized by crack-stretching of metallized track-etched membranes, J. Chem. Phys. 156 (3) (Jan 21 2022) 034902, https://doi.org/10.1063/5.0078451.
[36] N.P. Kovalets, I.V. Razumovskaya, S.A. Bedin, A.V. Naumov, Giant Raman scattering on plasmon metal surfaces as a method to control their functional and supramolecular structural characteristics, JETP Lett. 118 (4) (2023) 249–254, https://doi.org/10.1134/s0021364023602233.
[37] N.P. Kovalets, S.A. Bedin, I.V. Razumovskaya, A.V. Naumov, Giant Raman Scattering of Light as a Way to Inspect Defects and Cracks Metal Coatings Dielectric Materials, Photonics Russia. 8 (8) (December 15 2023) 620–621, https://doi.org/10.22184/1993-7296.FRos.2023.17.8.620.621
[38] A. Prisacaru, O. Shikimaka, E. Harea, A. Burlacu, M. Enachi, T. Braniste, Nano- and microscratching as a potential method for texturing the Si surface, Moldavian Journal of the Physical Sciences (2014) 188–194.
[39] X. Rao, et al., Material removal mode and friction behaviour of RB-SiC ceramics during scratching at elevated temperatures, J. Eur. Ceram. Soc. 39 (13) (2019) 3534–3545, https://doi.org/10.1016/j.jeurceramsoc.2019.05.015.
[40] A.V. Golovanova, M.A. Domnina, A.I. Arzhanov, K.R. Karimullin, I.Y. Eremchev, A.V. Naumov, AFM characterization of track-etched membranes: pores parameters distribution and disorder factor, Appl. Sci. 12 (3) (2022) 1334 [Online]. Available: https://www.mdpi.com/2076-3417/12/3/1334.
[41] E.P. Kozhina, A.I. Arzhanov, K.R. Karimullin, S.A. Bedin, S.N. Andreev, A.V. Naumov, Using epi-luminescence microscopy to visualize and control the distribution of luminophores on a highly-developed surface, Bull. Russ. Acad. Sci. Phys. 85 (12) (2022) 1393–1399, https://doi.org/10.3103/s1062873821120169.
[42] F.X. Liu, et al., Micro-scratch study of a magnetron-sputtered Zr-based metallic-glass film, Surf. Coating. Technol. 203 (22) (2009) 3480–3484, https://doi.org/10.1016/j.surfcoat.2009.05.017.
[43] I.V. Razumovskaja, L.L. Muhina, G.M. Bartenev, About the mechanism of inorganic glass deformation during the microindentation, Reports of USSR Academy of Science 213 (4) (1973) 822–825.
[44] A.I. Arzhanov, A.O. Savostyanov, K.A. Magaryan, K.R. Karimullin, A.V. Naumov, Photonics of Semiconductor Quantum Dots: Basic Aspects, Photonics Russia. 15 (2021) 622, https://doi.org/10.22184/1993-7296.FRos.2021.15.8.622.641
[45] K.R. Karimullin, A.I. Arzhanov, I.Y. Eremchev, B.A. Kulnitskiy, N.V. Surovtsev, A.V. Naumov, Combined photon-echo, luminescence and Raman spectroscopies of layered ensembles of colloidal quantum dots, Laser Phys. 29 (12) (2019/10/25 2019) 124009, https://doi.org/10.1088/1555-6611/ab4bdb.
[46] V.V. Klimov, Control of the emission of elementary quantum systems using metamaterials and nanometaparticles, Physics Uspekhi. 64 (2021) 990–1020, https://doi.org/10.3367/UFNe.2021.01.038910.